Stall Flutter Instabilities on the IEA-15 Reference Wind Turbine in Idling Conditions : Code-to-Code Comparisons and Physical Analyses

J. Loubeyres, J.-L. Pfister, F. Blondel, N. Guy

Stall flutter instabilities on the IEA-15 reference wind turbine in idling conditions: code-to-code comparisons and physical analyses

Stall flutter instabilities on the IEA-15 reference wind turbine in idling conditions: code-to-code comparisons and physical analyses

J. Loubeyres[1], J.-L. Pfister[1], F. Blondel[1], N. Guy[1]

[1]IFP Energies nouvelles, 1-4 avenue de Bois Préau, 92852 Rueil-Malmaison, France.

Author contact email: `jean-lou.pfister@ifpen.fr`

Abstract The present study investigates stall-induced vibrations on a IEA-15-RWT wind turbine blade. At standstill and under specific strong crosswind conditions, simulations using the codes OpenFAST and DeepLines Wind^{TM} exhibit large-amplitude vibrations. Results of both codes are first compared, showing an overall good agreement. Then, the influence of the wind misalignment angle is assessed as well as the choice of aerodynamic polar datasets. Vibrations are observed within two well-marked angular sectors, and the high sensitivity of the phenomenon to the choice of polars is highlighted. Finally, a simplified model based on a spring-mounted aeroelastic section is used to help identifying which type of unstable aeroelastic modes may be at play.

Keywords: IEA-15-240-RWT, aeroelasticity, stall flutter, OpenFAST, DeepLines Wind^{TM}

1. Introduction

Some reference wind turbines (RWT) are made publicly available for open research and technology development in the field of wind energy. In contrast to commercial wind turbines subject to confidentiality clauses, these virtual reference models allow the development and comparison of methods based on freely accessible designs. The ongoing trend for increasing offshore wind turbine size has recently led the International Energy Agency (IEA) Wind Technology Collaboration Platform (TCP) to the definition of a new reference design, rated at 15 MW for a 240 m wide rotor [1] (referred to as IEA-15 in what follows), paving the way for the development of next-generation offshore wind turbines.

Among the issues raised by the increase in size of these new generation wind turbines is the aeroelastic behaviour, which poses challenges both in terms of modelling and design. Earlier studies [2, 3, 4, 5, 6, 7] have reported and analysed the occurrence of stall-induced vibrations of wind turbine blades in idling conditions subject to a misaligned wind. These vibrations arise when the loss of lift and/or the unsteady loads resulting from the aerodynamic stall (caused by the misalignment of the blades with respect to the incoming wind) interact unfavourably with the mechanical structure of the blades [7], leading eventually to large-amplitude vibrations. Practically, this phenomenon may happen in case of strong winds (in which case the rotor is stopped for safety reasons) if the nacelle orientation system fails. In this case, there is no longer any possibility to align the blades with the wind.

The IEA Wind 15 MW RWT appears to be a relevant case study, useful to both industry and researchers, to challenge modelling and design methods related to the aeroelastic behaviour of wind

turbine blades. The current work focuses on the modelling of the IEA-15 wind turbine in idling conditions, subjected to a strong crosswind representative of extreme environmental conditions. With some surprise, the authors of this note observed that the original design of the IEA-15 wind turbine seems to be particularly responsive to stall flutter instabilities.

The objectives of the present work are then twofolds: in a first part, we assess the occurrence of the stall flutter phenomenon in the case of the IEA-15 design using two different simulation codes. This allows evaluating to which extent standard codes can reliably reproduce this instability. Since the considered cases involve very large displacements of the blades, we are in a configuration notably more difficult to simulate than more conventional operating conditions. In a second part, the phenomenon is analysed from a more physical perspective. The dependence to parameters is investigated, then a simplified model is used to clarify the mechanisms at play.

2. Code-to-code comparisons of the blade response

The 15-MW IEA reference wind turbine is used for all the benchmarks performed within this study. Since our main focus is on aeroelasticity, the fixed offshore version of the turbine has been considered, without the influence of hydrodynamics. In addition, for the sake of simplicity, we consider only *one isolated blade* of the turbine, which is clamped at its root position. A sketch of one blade section is reported in Figure 1, where axis x is oriented in the flapwise direction (with a small angle offset due to the blade twist), axis y the edgewise direction and axis z is oriented along the elastic axis of the blade (directed towards the tip). The angle between the wind direction and the global y axis is noted γ. No controller dynamics is considered. Note that this simplified configuration is not particularly restrictive considering the physics involved: simulations of the complete turbine showed similar behaviour to that presented in the following [8].

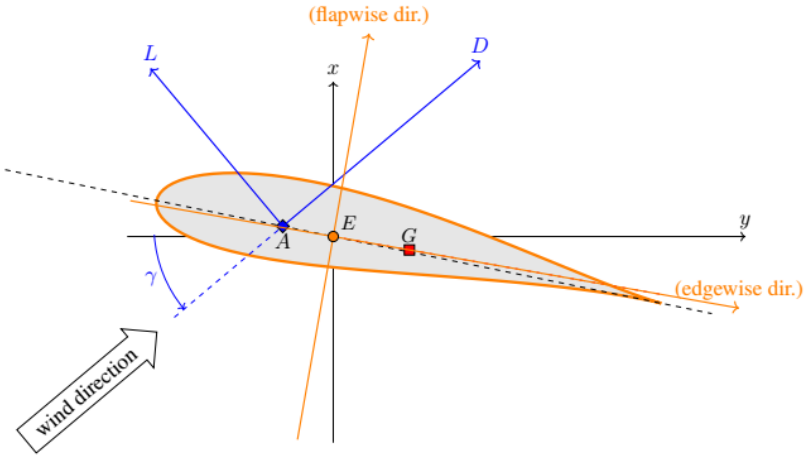

Figure 1. Sketch of one airfoil section of the blade, with typical positions of the aerodynamic centre A, elastic centre E and mass centre G. The prebend of the blade is directed towards the negative x direction, and the airfoil is showed here with initial twist (chordline not aligned with y axis).

The open-source code OpenFAST v3.0.0[1] as well as the commercial software DeepLines Wind^{TM} v5.6.3[2] have been used for the computations, allowing code-to-code comparisons and cross-validations. DeepLines Wind^{TM} [9] is an aero-hydro-servo-elastic multibody solver, capable of simulating complete (floating) wind turbine systems, including horizontal and vertical axis wind turbines. Within this software, mechanical parts are modelled as non-linear beam elements, while

[1] `https://www.nrel.gov/wind/nwtc/openfast.html`
[2] `http://www.principia-group.com/blog/product/deeplines-wind/`

various aerodynamics models are available as external libraries. OpenFAST is an open-source computational framework that couples various modules developed for the simulation of the dynamic, coupled response of (floating) wind turbines. Specifically, we have used the structural model BeamDyn, coupled to the aerodynamics module AeroDyn.

In the following, we first describe the modelling of the blade and the aerodynamics within both codes. Then, pure steady and unsteady mechanical calculations, i.e., without aerodynamics, are performed. Finally, a representative coupled aeroelastic simulations are described and compared to an analytical model.

2.1. Models description

2.1.1. Blade structural model Both BeamDyn and DeepLines are based on beam models allowing for large displacements and rotations. The salient features of each solver are recalled in the following.

- *DeepLines Wind^{TM}*: the modelling of all structural elements is based on a geometrically exact beam theory very similar to that proposed by Simo and Vu-Quoc [10]. The solver can therefore handle composite beams with initial twist and curvature, having sectional material properties involving the definition of 6×6 mass and stiffness matrices whose coefficients vary along the span. Modal (over a statically pre-loaded configuration) and time-stepper analyses are available. For the latter, an implicit Newmark scheme is used for time integration, while a Newton loop (with exact Jacobians) is called at each time step to solve the mechanical equilibrium.
- *OpenFAST (BeamDyn)*: the high-fidelity solver BeamDyn is also based on a geometrically exact beam theory, written in a mixed form [11]. Overall, it has quite the same modelling scope (large displacements, geometry with initial deformations, 6×6 sectional properties) as DeepLines. The time-integration scheme is also similar. However the spatial discretization is quite different, since BeamDyn relies on a spectral method [11].

We have considered the original material and geometrical properties of the IEA-15 blade (sections with structural twist, elastic centre - shear centre offset, but no bend-twist couplings, geometry with twist and prebend). The blade is discretized with 50 sections for pure mechanical computations, and with 25 sections for aeroelastic calculations. A small and uniform (10^{-3}) Rayleigh material damping is considered. Gravity is set to zero.

2.1.2. Aerodynamics The standard aerodynamic models for wind turbine design are based on the blade element momentum theory [12]. In the present case, the blade is not rotating and hence wake effects are negligible. The "momentum" part of the method can therefore be discarded and the computation of the aerodynamic forces simply amounts to integrating the local drag, lift and moment coefficients along the span. Given the local angle of attack, these quantities can be obtained from pre-computed look-up tables. We consider two sets of data, both of which span the $[-180°, 180°]$ range of angle of attack (see Figure 2):

- Original blade data, which was obtained from the official IEA-15 repository[3]. These polar data have been obtained using the RANS solver Ellipsys2D, then modified with Du-Sellig 3D stall delay correction [13]. More precise details of the CFD and extrapolation methods used can be found in Gaertner et al. [1, §2.1].
- A set of polar data computed with the open-source finite-volume RANS code SU2[4] in the angle of attack range $[-40°; +40°]$ with an angle step of $2°$. The unsteady, two-dimensional flow was solved with the incompressible solver available in SU2, using a k–ω SST turbulence model. The boundary layer on the profiles was considered as fully turbulent, i.e., no transition model was considered. No wall-laws were applied for the boundary layer, with the first cell satisfying $y+ < 1$. The polar data was then calculated by averaging the aerodynamic coefficients after

[3] `https://github.com/IEAWindTask37/IEA-15-240-RWT`
[4] `https://github.com/su2code/SU2`

fitting their temporal variations with a cosine law. The obtained polars were then extrapolated over the full angle of attack range with AirfoilPreppy[5]. The polars were calculated for 8 airfoils sections, then extrapolated along the spanwise direction whenever needed. No stall-delay corrections are applied.

The polars obtained with SU2 are significantly different from the original polars (Ellipsys2D). On SU2 polars, important differences are observed between the different sections. Non-monotonic variations are present in the range 20°–40°: when the angle of attack reaches the stall point, the lift coefficient first decreases, but contrary to Ellipsys2D polars, it then either stagnate or increases until approximately 40°. This feature is also observed on most of the polar data available in the literature for beyond-stall angles of attack [14, 15]. Since stall flutter notably depends on the lift *slope*, this is expected to have a significant impact. The second important difference between the two data sets is related to the maximum lift coefficient: it is significantly higher with Ellipsys2D polars, which is likely due to the Du-Selig correction. Note that in the present study, since the turbine is in parked conditions and the blades are stopped, this stall delay correction is no longer really appropriate.

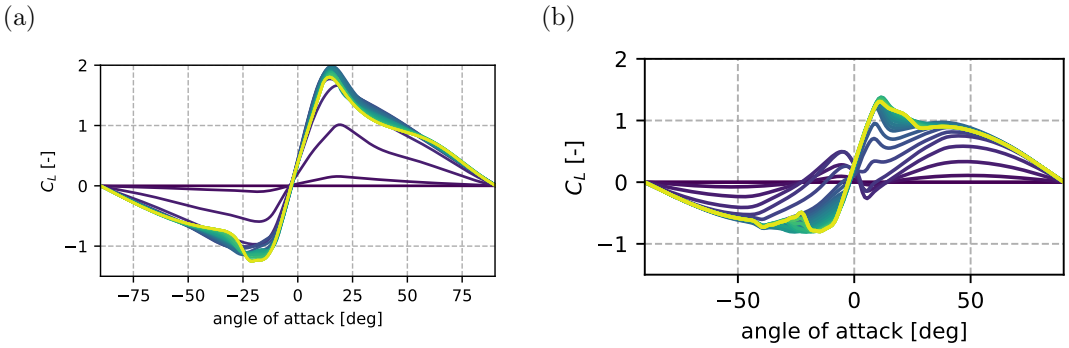

Figure 2. Polar data computed (a) with Ellipsys2D and Du-Sellig correction, and (b) with SU2 without any 3D correction. The data corresponding to 15 airfoils sections evenly distributed along the span are represented (the colour becomes lighter as one moves towards the tip of the blade).

Although dynamic stall models certainly have a strong influence on stall-induced vibrations, no such model is considered here. These models indeed involve tuning parameters that are hard to determine if no experimental data is available. Moreover, these models generally add damping to the system and have a stabilizing role [3, 6]. The case without dynamic stall thus probably allows to determine safe stability margins. Similarly, for the sake of simplicity, only steady wind conditions are considered here. More precisely, a wind ramp from zero to 45 m/s is prescribed during the first 100 seconds, then a constant wind of 45 m/s is prescribed for the rest of the simulation.

2.2. Steady blade mechanics computations

To assess the static behaviour of the blade, point-load equilibriums are computed: in both codes, tip loads in the global x (flapwise), y (edgewise) and z (axial) directions are applied. These loads are applied at the elastic centre of the tip section. The results are shown in Figure 3, showing a good agreement between DeepLines (DL) and BeamDyn (BD). We observe small but non-zero off-diagonal responses, i.e., a loading along one direction provokes a displacement along the orthogonal directions. This behaviour is mainly due to two effects. On one hand, the blade is curved and twisted, meaning that a tip load may induce distributed twisting moments and shear forces along the blade. On the other hand, because the shear centre of each section is not coincident with the elastic axis, the sectional matrices are not diagonal even in the principal bending frame. This reflects the presence of shear-twisting material couplings.

[5] `https://github.com/WISDEM/AirfoilPreppy`

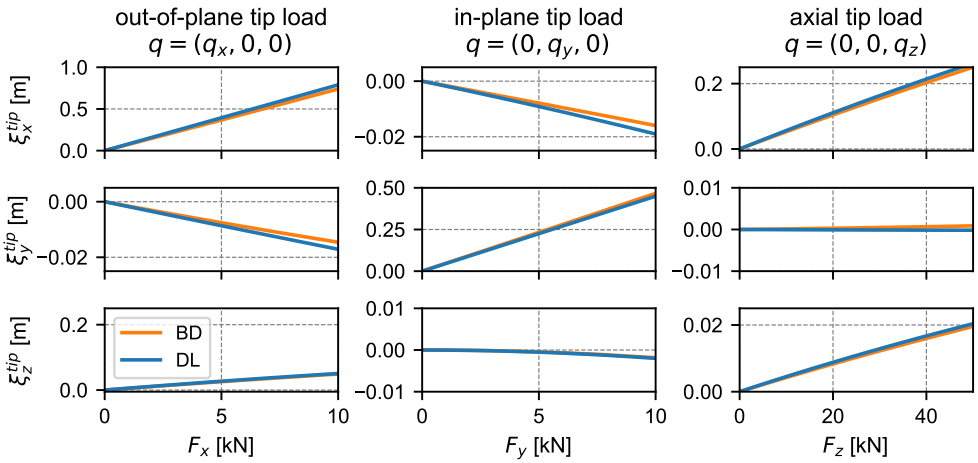

Figure 3. Steady point-load equilibrium calculation results. Steady tip displacement ξ^{tip} in global x, y and z directions, as a response of a concentrated point load applied at the tip of the blade in x (out-of-plane), y (in-plane) and z (axial) direction. The blue curve corresponds to DeepLines results and the orange curve to BeamDyn results.

2.3. Unsteady blade mechanics computations

The unsteady mechanical response of the blade to tip loads is considered here. A concentrated force of 100 kN is applied at the elastic centre of the blade's tip section, along global axes x and y, from $t = 0$ and maintained throughout the simulation. The tip displacement is then monitored along global x and y directions, resulting in a 4×4 time-displacement matrix shown in Figure 4-(a). The associated frequency spectrum is shown in Figure 4-(b). For both solvers, the time-step is set to 0.01 s. We observe a reasonable agreement between DeepLines (DL) and BeamDyn (BD). There is a very good match during the first five seconds, then the agreement progressively degrades. In

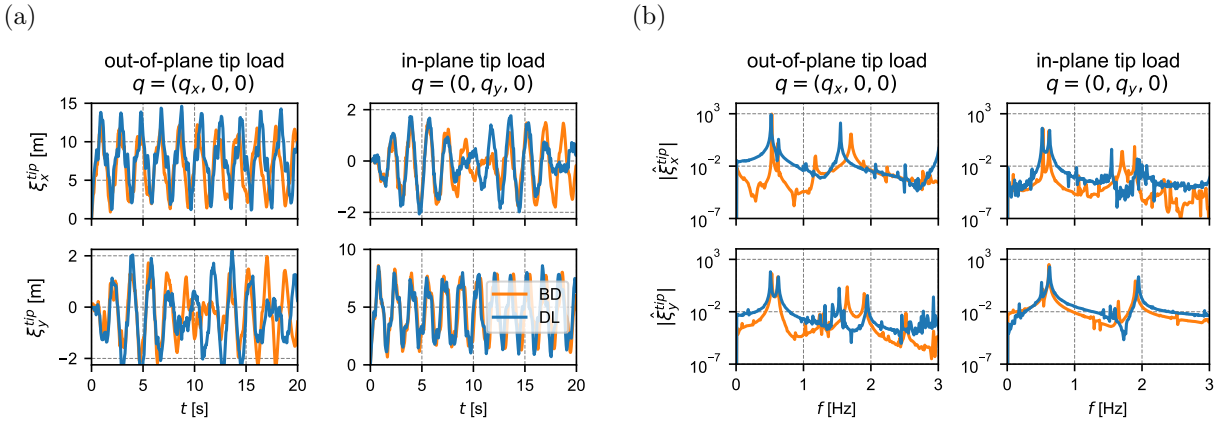

Figure 4. Unsteady point-load calculations. (a) unsteady tip displacement ξ^{tip} in global x, y and z directions and (b) associated frequency spectrum, as a response of a concentrated point load applied at the tip of the blade in x (out-of-plane), y (in-plane) and z (axial) direction. The blue curve corresponds to DeepLines Wind$^{\text{TM}}$ results, while the orange curve to BeamDyn results.

particular, as can be seen in (b), the two first frequencies of the blade (flapwise frequency at 0.523 Hz and edgewise frequency at 0.610 Hz) are in good agreement. These frequencies are slightly different

from what is indicated in the IEA report [1, p.8], but are in good agreement with the code-to-code comparison by Kim et al. [16] where the flapwise mode is found at 0.525 Hz.

2.4. Unsteady blade aero-mechanics computations

Let us now consider a coupled aero-elastic case. The wind speed is set to 45 m/s, and the misalignment angle γ to $-40°$. For this value of γ, the blade is in stalled conditions. The coupled response is computed using DeepLines Wind^{TM} coupled to the BEM model AeroDeeP on one hand, and using BeamDyn coupled to AeroDyn through OpenFAST on the other hand. With DeepLines Wind^{TM}, an automatic time-step strategy is adopted, which results in time-step of the order of 0.04 s. Because of the current limitations of OpenFAST/BeamDyn dynamic coupling capabilities, a much smaller time-step of 0.001 s had to be considered. In addition, it is worth noting that many simulations blew out for quite unexpected reasons. A workaround was (i) to vary the spectral order of the elements used within BeamDyn (BeamDyn key `order_elem` varied between 3 and 10) — this was not, however, a very satisfactory method, since it may influence the results — and (ii) to increase the number of sub-iterations between OpenFAST modules (`NumCrctn` key).

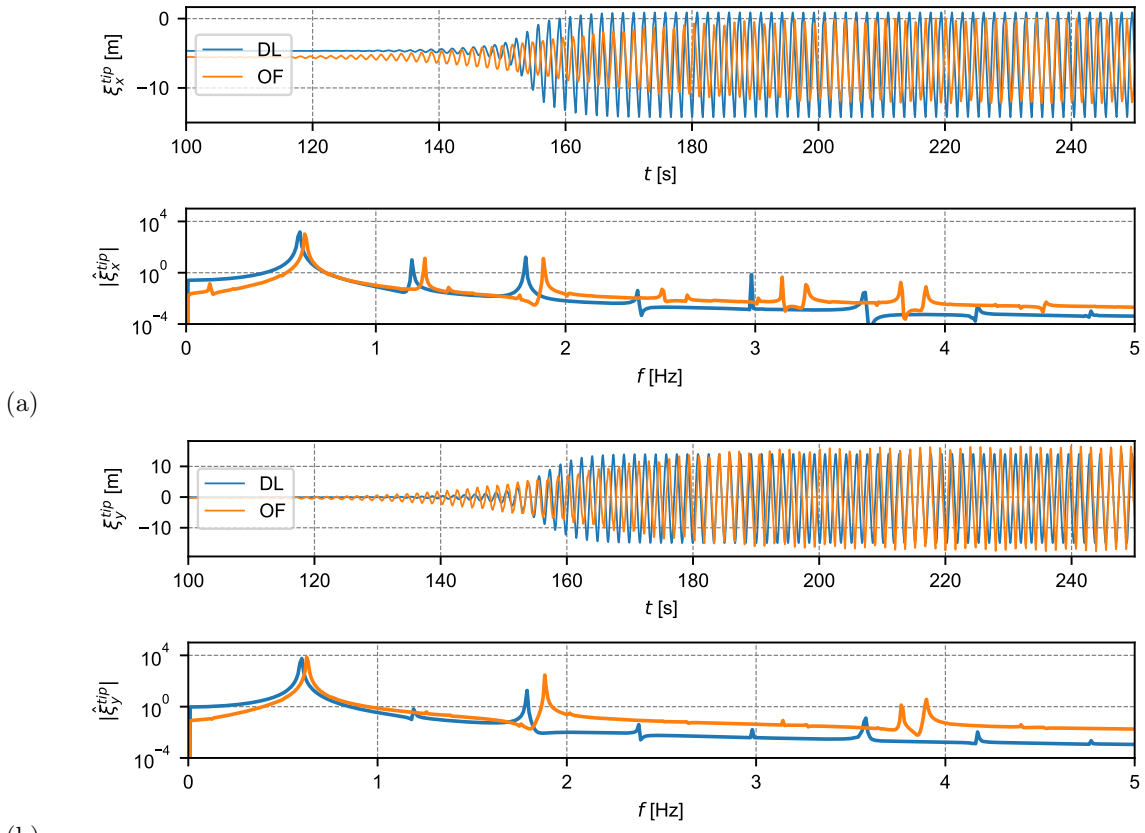

Figure 5. Unsteady aeroelastic calculation. For a misalignment angle of $-40°$, representation of the timeseries (top) and frequency spectra of the limit-cycle oscillations (bottom) for (a) the blade tip x displacement (flapwise direction) and y displacement (edgewise direction).

The blade's tip displacement in the flapwise (x) and edgewise (y) directions is reported in Figure 5, where DeepLines Wind^{TM} (DL) and OpenFAST (OF) results are superimposed. For both cases, a quasi-steady displacement is first observed, then the sudden development of very large-amplitude oscillations from $t \simeq 140$ s appears. A large displacement of the blade towards $x < 0$ is observed, because the resultant of the aerodynamic force (lift/drag) is primarily negative and along x axis.

In terms of vibration amplitudes, a very good agreement is observed in the edgewise direction, even if the amplitude is greater than 20 m. A less good agreement is observed in the flapwise direction. As can be observed in the frequency spectra, there is a good match in terms of lower vibration frequency, which is found to be close to that of the first edgewise vibration mode. The gap between DL/OF frequencies, on the other hand, increases greatly as one move towards the higher frequencies of the spectrum.

3. Stall-induced vibrations of the IEA-15-RWT

In the rest of the paper, we consider only the DeepLines Wind^{TM} model of the blade.

3.1. Parametric study

A set of aeroelastic simulations have been carried out, covering a range of misalignment angles $\gamma \in [-90°, 90°]$ and a period of 500 s, using the original and SU2 polar data. In both cases, there is a range of misalignment angles for which large-amplitude vibrations are observed. A summary of the main results obtained is given in Figure 6.

Let us first describe the results obtained with the original polar data — Figure 6-(a). The tip displacement magnitude is reported on top, with the min/max in solid line and the average displacement in dashed line. These quantities are calculated as averages over the 100 last seconds of the simulation (for all cases exhibiting large-amplitude vibrations, the limit-cycle is then reached). Unstable regions are observed for $\gamma \in [-52°, -16°]$ and $\gamma \in [10°, 83°]$. These unstable regions are associated with an important mean displacement that can reach more than 20 m, and large-amplitude fluctuations. A larger unstable region is present at positive geometric angles of attack, $\gamma > 0$, compared with the negative geometric angles of attack case, $\gamma < 0$. It can be, at least partially, attributed to the camber of the airfoil. Note also how sharp is the "high-angle-of-attack" transition region (at $\gamma \simeq -52°/+83°$), compared to the other unstable/stable threshold where the vibration amplitude varies smoothly as γ is varied. The frequency spectrum is shown on the graph at the bottom (only when oscillations are observed). Frequency peaks appear there in blue colour. The lowest oscillation frequency is found close to that of the first edgewise mode of the blade (0.61 Hz).

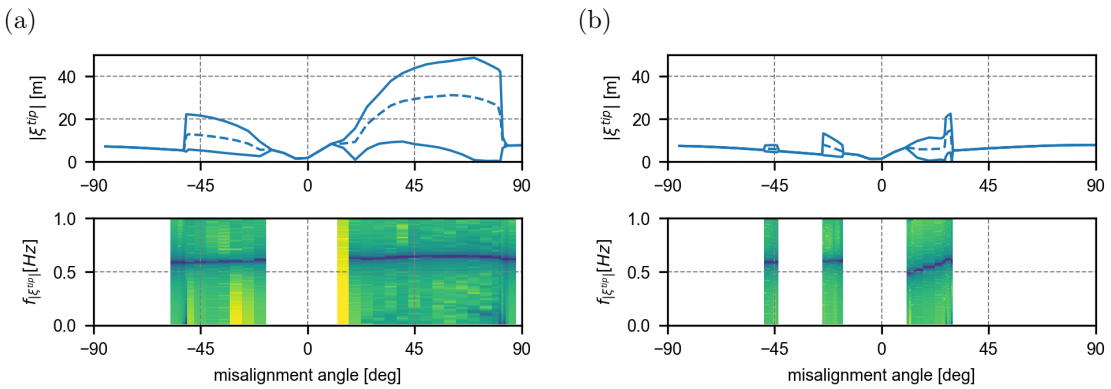

Figure 6. Effect of the misalignment angle on the stall flutter vibrations. For (a) original polar data and (b) SU2 polar data, representation of the minimum/maximum and mean vibration magnitude of the blade tip (top) and spectrum of the blade tip vibration magnitude (bottom).

As can be observed in Figure 6-(b), the model with SU2 polar data results in much reduced stall-induced vibrations, both in amplitude and range of "dangerous" wind directions. This shows once again how the results of the blade element methods are sensitive to the polar data.

3.2. Analysis of an equivalent aeroelastic section

To better understand the mechanisms at play in the observed instability, we consider a simplified model, consisting of a single airfoil section mounted on two linear and one rotational spring (the section rotates about the elastic axis E by an angle θ, and experiences translations about axes x and y). We note the generalized coordinate $\boldsymbol{q}(t) = [x(t), y(t), \theta(t)]^T$. A complete description of this kind of model can be found e.g. in Stäblein et al. [17]. The aerodynamic forces — drag, lift and pitching moment projected onto the generalized coordinates — are considered on their simplest form (i.e. without considering Theodorsen theory). They are then quasi-static and only depends on the instantaneous angle of attack, which itself depends on position $\boldsymbol{q}$ and velocity $\dot{\boldsymbol{q}}$. Their exact expression is obtained from the same look-up table as those used in the previous calculations. The application of Lagrange's equations gives an evolution equation that can be further linearized to study the small-amplitude vibrations about the position $\boldsymbol{q} = \boldsymbol{0}$. Vibration modes $\boldsymbol{q}'(t) = \hat{\boldsymbol{q}} \exp(\lambda + 2\pi f)t$ can be then obtained by solving an eigenvalue problem of type

$$\Big[(\lambda + 2\pi f)^2 \mathbf{M}_s + (\lambda + 2\pi f)\big(\mathbf{C}_s - \mathbf{C}_a\big) + \big(\mathbf{K}_s - \mathbf{K}_a\big)\Big]\hat{\boldsymbol{q}} = \boldsymbol{0} \tag{1}$$

where $\mathbf{M}_s$, $\mathbf{K}_s$ and $\mathbf{C}_s$ are the structural Jacobian matrices, and $\mathbf{C}_a$ and $\mathbf{K}_a$ are aerodynamic added-damping and added-stiffness matrices. The explicit expressions of these matrices are quite cumbersome in the general case, for that reason they were determined using the symbolic differentiation capabilities of the Python library `Sympy`.

There is *a priori* no direct link between this "section-wise" model and the behaviour of the complete IEA-15 blade. In order to relate this simplified model to the overall blade model, it is assumed that the spring stiffness coefficients k_x, k_y and k_θ are such that the corresponding natural frequencies coincide with the first flapwise, first edgewise and first torsional frequency of the *complete* blade, as determined by modal analysis of the blade performed using DeepLines Wind$^{\text{TM}}$. The damping coefficients are taken (quite arbitrarily) to small values of 10^{-3}. The other sectional coefficients — mass per unit length, chord length, distances between the elastic axis and aerodynamic centre and mass centre, and polar data for lift, drag and moment as a function of the angle of attack — are the same as those considered for the complete model. It is then possible to compute, as a function of the misalignment angle γ and the spanwise position z along the blade, the vibration eigenmodes of the "equivalent" spring-mounted airfoil section. Since the model has three degrees of freedom, three vibration modes are obtained, among which some may be unstable ($\lambda > 0$).

The results are reported in Figure 7, where coloured regions indicate the presence of an unstable mode. For the case (a) — original polar data — it is observed that there are unstable modes of moderate growth-rate roughly in the regions where the *entire blade* exhibit instabilities (the limits of the two unstable regions observed in Figure 6-(a) are marked there with the black solid and dashed lines). A typical mode shape ($\gamma = 25°$, tip section) for the most unstable mode in this region is represented in Figure 8-(a). For this mode $\lambda = 1.14$ and $f = 0.51\,\text{Hz}$, and the motion is a combination of flapwise and edgewise displacements. This is in qualitative agreement with what is observed in aeroelastic simulations of the entire blade. On the other hand, we see that all blade sections beyond a radius of 75m, in the region close to $\gamma = 0$, exhibit a very unstable mode ($\lambda > 5$, dark green colour). This mode is of different nature though. A typical unstable mode shape in this region is represented in Figure 8-(b), where we observe a classical flutter motion (combination of heaving/pitching motion). This mode is therefore clearly related to the classical coupled-mode flutter mechanism occurring at small angles of attack and high inflow velocity. All other modes are stable in this region, including the "stall flutter mode" described above. For some reason, it seems that although some parts of the blade are unstable with respect to classical flutter, this has no effect on the global dynamics of the blade.

Finally, the same analysis has been conducted on the case with SU2 polars. For this case it is harder to make a straightforward link between the sectional analysis and the global behaviour of the blade. Unstable regions as observed on the full-blade simulation are delimited using the black solid, dashed and dotted line, and we see that there are many other regions in the graph where

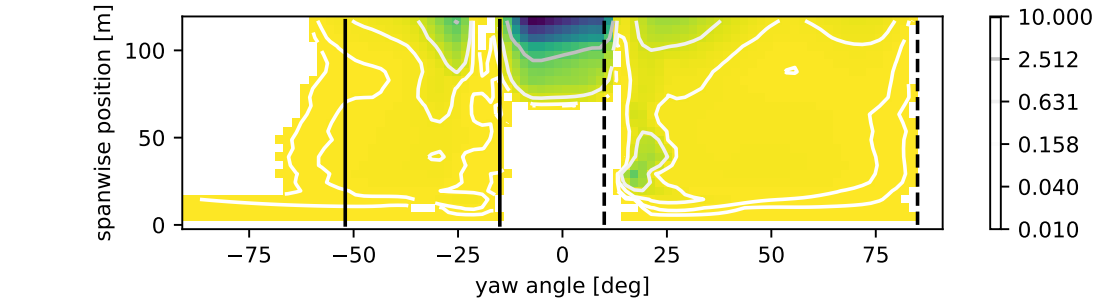

(a)

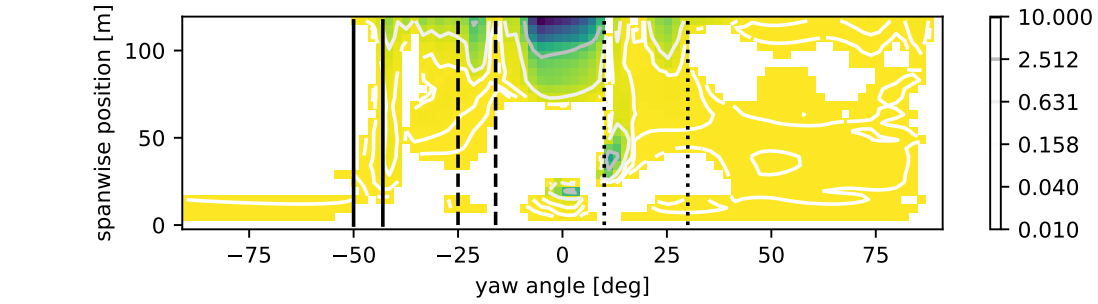

(b)

Figure 7. Local aeroelastic stability analysis along the blade span, for (a) original polar data and (b) SU2 polar data. Coloured area indicate the presence of an unstable mode (darker means more unstable), while white area indicate regions where all modes are stable. Black lines indicate the limits of the unstable regions as obtained from the full aeroelastic simulations.

(a) (b)

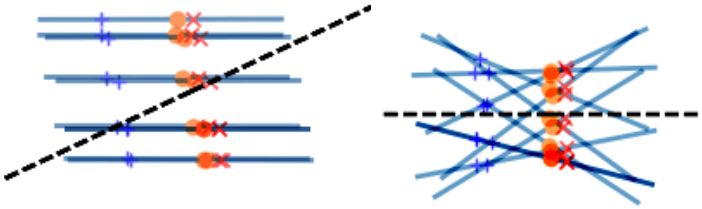

Figure 8. Snapshots of the deformation of the airfoil section of the most unstable mode for (a) $\gamma = 25°$ and (b) $= 0°$, for the case with original polar data and the tip airfoil section. The blue cross identifies the aerodynamic centre, the orange dot the elastic centre and the red cross the centre of mass, while the chordline is sketched with the blue line. The dashed line indicates the wind direction (from left to right)

unstable modes are found. Like previously, the very unstable modes in the region in the vicinity of $\gamma = 0$ are classical flutter modes.

In any case, it is intersting to observe that it is to some extent possible to make a link between the local (i.e. sectionwise) aeroelastic stability properties of each blade sections, and the global behaviour. In particular, we clearly see that a combined edgewise/flapwise mode becomes unstable because of the stalled condititions of the flow.

4. Conclusion

An isolated IEA-15-RWT blade subject to extreme wind conditions has been studied in this work, in configurations where severe stall flutter vibrations can occur. We have first performed code-to-code comparisons between DeepLines Wind^{TM} and OpenFAST (BeamDyn/AeroDyn), showing that both codes are in good agreement. Nevertheless, it is observed that the coupling strategy implemented at this stage within OpenFAST has some limitations in terms of time-step (convergence required time-steps 40 times smaller compared to DeepLines Wind$^{\mathrm{TM}}$) and/or overall convergence. We hope that the comparisons presented here may help for the development of improved versions of OpenFAST.

We have also shown how sensitive is the stall flutter phenomenon with respect to the polar data used in the calculations, and proposed a link between the behaviour of the full three-dimensional blade configuration and "local" vibration modes of equivalent spring-mounted airfoil sections distributed along the span. This may open the possibility of section-wise aero-structural optimizations aiming at improving the overall blade performance.

An obvious way to enrich this work would be to study the impact of dynamic stall models on the behaviour of the blade, calibrated on resolved CFD calculations, or even perform resolved fluid-structure computations over this configuration. The value of the "section-wise" approach for the prediction of unstable regions is also to be assessed more toroughly.

Acknowledgments The authors wish to thank Yann Poirette and Vincent Le Corre for their contribution in IEA-15-RWT modelling and help in the identification of the test case studied herein.

References

[1] E. Gaertner, J. Rinker, L. Sethuraman, F. Zahle, B. Anderson, G. Barter, N. Abbas, F. Meng, P. Bortolotti, W. Skrzypinski, G. Scott, R. Feil, H. Bredmose, K. Dykes, M. Sheilds, C. Allen, and A. Viselli, "Definition of the IEA 15 MW Offshore Reference Wind Turbine," NREL/TP-75698, International Energy Agency, Tech. Rep., 2020. [Online]. Available: https://www.nrel.gov/docs/fy20osti/75698.pdf

[2] K. Wang, V. A. Riziotis, and S. G. Voutsinas, "Aeroelastic stability of idling wind turbines," *Wind Energy Science*, vol. 2, no. 2, pp. 415–437, 2017.

[3] W. Skrzypiński and M. Gaunaa, "Wind turbine blade vibration at standstill conditions—the effect of imposing lag on the aerodynamic response of an elastically mounted airfoil," *Wind Energy*, vol. 18, no. 3, pp. 515–527, 2015.

[4] F. Zou, V. Riziotis, S. Voutsinas, and J. Wang, "Analysis of vortex-induced and stall-induced vibrations at standstill conditions using a free wake aerodynamic code," *Wind Energy*, vol. 18, no. 12, pp. 2145–2169, 2015.

[5] W. R. Skrzypiński, M. Gaunaa, N. Sørensen, F. Zahle, and J. Heinz, "Self-induced vibrations of a du96-w-180 airfoil in stall," *Wind Energy*, vol. 17, no. 4, pp. 641–655, 2014.

[6] T. Buhl, "Edgewise vibrations in stand still," Risø National Laboratory, Tech. Rep. Risoe-R No. 1611, 2006.

[7] M. H. Hansen, "Aeroelastic instability problems for wind turbines," *Wind Energy: An International Journal for Progress and Applications in Wind Power Conversion Technology*, vol. 10, no. 6, pp. 551–577, 2007.

[8] J. Loubeyres, "Aeroelasticity of the large reference wind turbine IEA 15 MW," Master's thesis, ISAE Supaéro, 2021.

[9] C. Le Cunff, J. Heurtier, L. Piriou, C. Berhault, T. Perdrizet, D. Teixeira, G. Ferrer, and J. Gilloteaux, "Coupled floating wind turbine simulator based on nonlinear finite element

method: Part i-methodology," in *ASME 2013 32nd International Conference on Ocean, Offshore and Arctic Engineering*, vol. 8, 2013.

[10] J. C. Simo and L. Vu-Quoc, "On the dynamics in space of rods undergoing large motions—a geometrically exact approach," *Computer methods in applied mechanics and engineering*, vol. 66, no. 2, pp. 125–161, 1988.

[11] Q. Wang, M. A. Sprague, J. Jonkman, N. Johnson, and B. Jonkman, "Beamdyn: A high-fidelity wind turbine blade solver in the fast modular framework," *Wind Energy*, vol. 20, no. 8, pp. 1439–1462, 2017.

[12] M. O. Hansen, *Aerodynamics of wind turbines*. Routledge, 2015.

[13] Z. Du and M. Selig, "A 3-d stall-delay model for horizontal axis wind turbine performance prediction," in *1998 ASME Wind Energy Symposium*, 1998, p. 21.

[14] P. Fuglsang, I. Antoniou, and H. Aagaard Madsen, "Wind tunnel tests of the FFA-W3-241, FFA-W3-301 and NACA 63-430 airfoils," Forskningscenter Risoe, Tech. Rep. Risoe-R No. 1041, 1998.

[15] R. E. Sheldahl and P. C. Klimas, "Aerodynamic characteristics of seven symmetrical airfoil sections through 180-degree angle of attack for use in aerodynamic analysis of vertical axis wind turbines," Sandia National Labs., Albuquerque, NM (USA), Tech. Rep., 1981.

[16] T. Kim, A. Natarajan, A. Lovera, E. Julan, C. Peyrard, M. Capaldo, G. Huwart, P. Bozonnet, and M. Guiton, "An extensive code-to-code comparison of a modified version of IEA15MW-UMaine floating wind turbine for H2020 HIPERWIND project," 2022.

[17] A. R. Stäblein, M. H. Hansen, and G. Pirrung, "Fundamental aeroelastic properties of a bend–twist coupled blade section," *Journal of Fluids and Structures*, vol. 68, pp. 72–89, 2017.